Computational Analysis of Dynamic SPK(S8)-JP-8 Fueled Combustor-Sector Performance

R. Ryder,[1] R.C. Hendricks,[2] M.L. Huber,[3] and D.T. Shouse[4]

[1]Flow Parametrics, LLC
68 Bushy Hill Road, Ivoryton, Connecticut 06442, USA
Phone: 860–767–0050, E-mail: ryderrc@comcast.net

[2]NASA Glenn Research Center, Cleveland, Ohio 44135, USA
[3]NIST, Boulder, Colorado 80305, USA
[4]AFRL/WPAFB, Wright-Patterson Air Force Base, Ohio 45433, USA
Work performed under US government - not subject to copyright in United States.

ABSTRACT

Civil and military flight tests using blends of synthetic and biomass fueling with jet fuel up to 50:50 are currently considered as "drop-in" fuels. They are fully compatible with aircraft performance, emissions and fueling systems, yet the design and operations of such fueling systems and combustors must be capable of running fuels from a range of feedstock sources. This paper provides Smart Combustor or Fuel Flexible Combustor designers with computational tools, preliminary performance, emissions and particulates combustor sector data. The baseline fuel is kerosene-JP-8+100 (military) or Jet A (civil). Results for synthetic paraffinic kerosene (SPK) fuel blends show little change with respect to baseline performance, yet do show lower emissions. The evolution of a validated combustor design procedure is fundamental to the development of dynamic fueling of combustor systems for gas turbine engines that comply with multiple feedstock sources satisfying both new and legacy systems.

INTRODUCTION

In prior computational fluid dynamics (CFD) combustion analysis work, Brankovic et al. (2007 and 2005), determined the theoretical performance of a trapped vortex combustor (TVC) fueled with a simulated coal-based (CTL) Fischer-Tropsch- (FT-) processed fuel derivative, synthetic paraffinic kerosene (SPK), that agreed well with experimental data. The term "hydroprocessed renewable jet" (HRJ) generally designates a fuel derived from biomass feedstocks. At that time the fuel itself was experimental and not all that well defined. However, sufficient spectral information was available to approximately simulate the fuel composition. By use of the NIST hydrocarbon database STRAPP (designation for Supertrapp), a 12-component mixture for the CTL SPK(JP-8) fuel was developed and specific heat C_p^0/R values extended to 4000 K by developing a two-parameter model for C_p^0/R based on the NASA thermophysical properties database (McBride et al., 2002) and the low-temperature values

generated by STRAPP. Caloric properties were also established for fuel blends of 30% and 70% synthetic fuel with JP-8. The analysis established caloric properties, specific heat, static enthalpy, and Gibbs free energy for the fuel mixtures of interest necessary for the CFD combustion analysis of the TVC. Fueling parameters used in that analysis are cited in the Appendix.

Currently alternate fuels such as FT- and biomass-derived fuels are covered under MIL-DTL-83133F and ASTM-D 7566 standards. Herein we use the STRAPP-NIST4 (Huber, 2007) and REFPROP (designation for REFPROP NIST23 (Lemmon et al., 2009)) databases.

The two-parameter temperature function model $C_p^0/R = A/T^{1/2} + B$, fitted to values of C_p^0/R in the domain 300–400 K to 600–800 K generated by STRAPP, was shown to adequately represent C_p^0/R and derived caloric properties H^0/RT, G^0/RT, S^0/R at temperatures of 2000–4000 K that are of interest for combustor engineering computations. The two-parameter model was shown to agree with selected components of the NASA thermophysical properties code away from saturation boundaries.

The caloric parameters presented by McBride et al. (2002) are given as Eqs. (1) to (7):

$$\frac{C_p^0(T)}{R} = \frac{a_1}{T^2} + \frac{a_2}{T} + a_3 + a_4 T + a_5 T^2 + a_6 T^3 + a_7 T^4 \qquad (1)$$

$$\frac{H^0(T)}{RT} = -a_1 T^{-2} + \frac{a_2 \ln T}{T} + a_3 + \frac{a_4 T}{2} + \frac{a_5 T^2}{3} + \frac{a_6 T^3}{4} + \frac{a_7 T^4}{5} + \frac{b_1}{T} \qquad (2)$$

$$S^0(T)/R = -\frac{a_1 T^{-2}}{2} - \frac{a_2}{T} + a_3 \ln T + a_4 T + \frac{a_5 T^2}{2} + \frac{a_6 T^3}{3} + \frac{a_7 T^4}{4} + b_2 \qquad (3)$$

From the fundamentals of thermodynamics, the Gibbs free energy and mixture internal energy are computed, respectively, as

$$\frac{G^0(T)}{RT} = \frac{H^0(T) - TS^0(T)}{RT} = \frac{H^0(T)}{RT} - \frac{S^0(T)}{R} \tag{4}$$

and

$$\frac{U^0(T)}{RT} \approx \frac{H^0(T)}{RT} \tag{5}$$

where

$$\frac{H^0(T)}{RT} = T^{-1} \int \left[\frac{C_p^0(T)}{R} \right] dT \tag{6}$$

and

$$\frac{S^0(T)}{R} = \int \frac{C_p^0(T)}{RT} dT \tag{7}$$

The approximating two-parameter model caloric forms are given as Eqs. (8) to (10) where C_1 and C_2 are integration constants:

$$\frac{C_p^0(T)}{R} = \frac{A}{T^{1/2}} + B \tag{8}$$

$$\frac{H^0(T)}{RT} = \frac{2A}{T^{1/2}} + B + \frac{C_1}{T} \tag{9}$$

$$\frac{S^0(T)}{R} = -\frac{2A}{T^{1/2}} + B\ln T + C_2 \tag{10}$$

The two-parameter model C_p^0/R is temperature- and fluid-dependent, and its integrated forms were selected because they have the proper asymptotic trends and are accurate enough to provide high-temperature caloric properties when based on accurate lowtemperature-based information such as derived from STRAPP.

While the two-parameter model Eqs. (8) to (10) are sufficiently accurate for combustor engineering computations, a more accurate representation of specific heat at "zero" pressure (C_p^0) at low temperatures near gas saturation boundaries or the liquid regime requires an equation of state or higher-order polynomial representation. However, higher degree polynomials often exhibit unpredictable behavior when extended outside the domain of fit for intended use, making this choice less desirable. The Planck-Einstein model for C_p^0/R developed by Yokozeki et al. (1998), provides a more accurate representation of C_p^0 in the low-temperature regimes, making the Planck-Einstein model a better choice for a source to generate the two-parameter model fit, which is then extended to combustor temperatures.

PLANCK-EINSTEIN MODEL FOR C_p^0

The Planck-Einstein functions are used by Huber et al. (2008a) and implemented into REFPROP as a more reliable method of calculating C_p^0 at lower temperatures, yet possess the proper trends at elevated temperatures that are not always provided by polynomials when extrapolated beyond their intended range of application.

$$C_p^0 = C_0 T^{C_1} + C_2 \frac{(C_3/T)^2 \exp(C_3/T)}{[1 - \exp(C_3/T)]^2} + C_4 \frac{(C_5/T)^2 \exp(C_5/T)}{[1 - \exp(C_5/T)]^2} + C_6 \frac{(C_7/T)^2 \exp(C_7/T)}{[1 - \exp(C_7/T)]^2} \tag{11}$$

where the temperature T is in K and C_p^0 is in J/(mol-K).

The two-parameter coefficients A and B from Eq. (8), can be determined by fitting the C_p^0/R values of Eq. (11) or equivalently those of REFPROP, which uses a similar Planck-Einstein form over the temperature domain 300–400 K to less than 1000 K.

DETERMINING $C_p^0/R = A/T^{1/2} + B$ FOR FUEL S8

Huber et al. (2008a, 2008b, and 2009) provide both the simulated composition (Table. 1) and the Planck-Einstein coefficients (Table. 2) representative of the GTL (gas to liquid) FT aviation fuel denoted as S8.

Planck-Einstein Eq. (11) provides the calculated or reference value of C_p^0 for each of the n_j fluid components in the mixture. Because linear mixing rules apply, the calculated or reference value C_p^0 S8 for the mixture S8 becomes

$$C_{pS8}^0 = \sum n_j C_p^0 \tag{12}$$

The two-parameter formulation is fitted to these results, providing the necessary two coefficients (A' and B') for S8:

$$C_{pS8}^0 = A'/T^{1/2} + B' \quad \text{J/(mol-K)} \tag{13}$$

where
- A' = −15202
- B' = 1097.8
- R = 8.314472 J/(mol-K)

and molar mass M = 164.79 kg/(k-mol). Integrating Eqs. (11) and (13), the caloric properties S_j^0 and H_j^0 are calculated for each component of the mixture in S8. Again, linear mixing rules are assumed to provide S_{S8}^0 and H_{S8}^0:

$$S_{S8}^0 = \sum n_j \left(S_j^0 - \ln n_{jj} \right) \tag{14}$$

$$H_{S8}^0 = \sum n_j H_j^0 \tag{15}$$

Planck-Einstein Model

$$\frac{H}{RT} = \frac{1}{T} \int \left(\frac{C_p^0}{R} \right) dT$$

$$= \frac{C_0 T^{C_1}}{R(C_1+1)} + \frac{\left[\left\{ \sum \frac{C_{2j+1}C_{2j}}{-1+e^{\frac{C_{2j}}{x}}} + \text{Constant} \right\} \right]}{RT}$$

(16)

$$\frac{S^0}{R} = \iint \left(\frac{C_p^0}{RT} \right) dT$$

$$= \frac{\left[\frac{C_0 T^{C_1}}{C_1} + \left\{ \sum \frac{C_{2j+1} C_{2j}/x}{\left(-1+e^{\frac{C_{2j}}{x}} \right)} - \log_e \left(-1+e^{\frac{C_{2j}}{x}} \right) + C_{2j}/x \right\} \right]}{R}$$

$$+ \frac{\text{Const}}{R}$$

(17)

Two-Parameter Model

Values for S_{S8}^0 and H_{S8}^0 are obtained directly by integrating the two-parameter formulation for C_{pS8}^0:

$$H_{S8}^0 = \int C_{pS8}^0 dT = 2A'T^{1/2} + B'T + C_1' \quad \text{J/mol} \qquad (18)$$

$$S_{S8}^0 = \int \frac{C_{pS8}^0}{T} dT = \frac{-2A'}{T^{1/2}} + B' \ln(T) + C_2' \quad \text{J/(mol-K)} \qquad (19)$$

where $C_2' = -7960$ J/(mol-K)
$C_1' = 191400$ J/mol

For consistency, the reference states, S_{S8}^{00} and H_{S8}^{00} are chosen to match that produced by the NIST Code REFPROP (2009). This reference state was selected at T= 400 K and "zero" pressure (P = 10^{-6} MPa).

$$H^{00} = 22448 \text{ J/mol}$$

$$S^{00} = 138.4 \text{ J/(mol-K)}$$

The two-parameter model constants for combustion computations within reasonable engineering accuracy for caloric properties C_p^0/R, $H^0/(RT)$ and S^0/R are given in Table. 3, with a comparison of values normalized to Jet A at 300 K given in Figs. 1a, b, and c, respectively. With these properties, other thermodynamic properties such as Gibbs and internal energies, follow.

Note: Conversion of integration constants for H^0/RT requires additional terms, and best practice is to work with dimensional forms, otherwise at a given RT, the value [H1 (1 − $H^0$1/H1)]/[H2(1−$H^0$2/H2)]] where 1 and 2 refer to H values determined by thermodynamic state points (T1, P1) and (T2, P2).

The coefficients A and B for C_p^0, for Jet A and S8 are similar, and one would not expect significant variations in combustion properties, yet somewhat higher combustor temperatures should be anticipated when compared with the synthetic fuel (GTL) simulation in the TVC combustor.

Liquid-phase fuel properties are also required to describe the initial injection of liquid-fuel spray droplets into the combustor through orifice injectors. The needed values for synthetic fuel (GTL) are from Brankovic et al. (2007) and values for S8 from REFPROP (Table. 4). Additional property values required for accurate spray droplet dynamics and evaporation rates include specific heat, viscosity, and thermal conductivity are also from REFPROP.

Combustion chemistry is modeled by use of the three-step reduced chemistry model of Molnar and Marek (2003), which consists of a fuel breakup and oxidation equation into CO and H_2O (Step 1), oxidation of CO into CO_2 (Step 2), and dissociation of N_2 and O_2 into NOx (Step 3). Previous validation studies (Hendricks et al., 2001 and 2004; and Brankovic et al., 2005 and 2007) provide useful information on injection conditions for the liquid fuel, including droplet diameter distributions, velocities, and spray cone angles. Fuel droplet dissociation is not modeled.

With the necessary thermophysical properties required by the flow solver, we now turn our attention to the combustor modeling and computations.

COMBUSTORS AND CFD MODELS

In the prior work of Brankovic et al. (2007) the Air Force Research Laboratory, Wright-Patterson Air Force Base (AFRL/WPAFB) trapped vortex combustor (TVC) sector rig was used as the experimental baseline for comparison of a variety of combustors.

TVC COMBUSTOR

For the TVC combustor geometry, there exists a wealth of validation data including, for example, wall pressures, emissions, and high-frame-rate video for flame structure. Further, the inlet diffuser and combustor geometries have been accurately described with computer-aided design (CAD), with known coolant flows and spray droplet characterizations. It is also well known that the TVC operates stably over a wide range of equivalence ratios and combustor pressures and has been useful in studies of altitude restart and lean blow out (LBO). A schematic of the test rig being simulated is shown in Fig. 2a, which illustrates the airflow and fuel injection sites as well as the general flow patterns expected within the combustor. Provision for addition of water mist for pollutant emission reduction studies is also indicated. A photograph of the combustor hardware is shown in Fig. 2b, with the sidewall removed for optical access. Components of the rig include the tripass diffuser, combustor bulkhead, heat shield, and combustor duct that exhausts to a vent. Combustor walls are cooled through effusion holes along the entire interior wall and film cooling through slots along the combustor upper and lower walls.

To evaluate different combustors, subsequent combustors will become generic by labeling them as A, B, C, etc., with ratios of combustor performance, emissions and fueling in order to provide comparisons without compromising proprietary concepts or geometric details. Herein results from combustor A will be presented. Evaluations for combustors B and C will be performed in a similar manner and published.

COMBUSTOR A

A CFD model was developed of combustor A to provide computations and interpretations of experimental work being carried out with the AFRL/WPAFB JP-8+100 in sector testing. These results will be applied to JP-8+100-fueled baseline combustor sector tests and to combustor sector tests by use of fuels (within MIL-DTL-83133F and ASTM-D 7566 specifications) including SPK-blends, biomass fuel blends, and green-jet blends over a range of equivalence ratio (φ), inlet pressure, and temperature including LBO (lean blow out). Combustor performance, stability, and emissions characteristics will be provided for and validated by the AFRL/WPAFB Combustor Sector Tests and data will be analyzed with the actual parametric values interactively determined in conjunction with NASA and AFRL.

Herein, we provide computations and interpretations of experimental test data including combustor emissions for a range of parametric conditions and for code validation based on AFRL experimental data.

The CAD model representation of the combustor required extensive cleanup in order to remove features not needed for the computational fluid analysis. Typically the CAD files are assembly files used in manufacturing that contain tolerances and gaps. These features result in the solid modeling to 'leak air'. The CAD changes consist of removing unnecessary features and modification so that the model 'holds air'. In addition, as only the combustion section was provided by CAD, a plenum was added in order to feed the combustor-sector. Figure 3 shows the finished CAD representation where only one-third of the sector is shown and the sliced side view between the fueling nozzles are shown in more detail in Fig. 4. Nozzle swirl vanes, nozzle tangential swirl holes, and combustor cooling holes provide for rapid mixing and fuel combustion as well as emissions control.

These sector geometries are quite complex. Even with experienced CAD cleanup, achieving a successful computational mesh is very laborious and not at all guaranteed. This configuration required 15 attempts and further CAD modifications before a successful computational mesh was produced.

The computation mesh was then ported to a set of parallel computational computers to test the computational mesh for consistency. Once the mesh was ruled to be a consistent mesh, within specified boundary conditions, the baseline hot flow could be computed.

Only three boundary conditions are required (Fig. 5): (1) the total air flow into the sector is specified at the inflow plane indicated by the black arrow, (2) the sector exit pressure is specified at the sector exit plane denoted by the red arrow, and (3) the fuel droplet specification. With these conditions in place, the sector calculations can be performed.

With a working model, the next stage is to set the fuel droplet specification and run the CFD analysis in parallel across eight computers. In this paper, the CFD results are compared against experiment for overall pressure loss and exit temperatures. Three fuels were analyzed: 0%, 50%, and 100% FT at three fuel:air ratios of 0.01, 0.015, and 0.02. The inlet pressure was 1.55 MPa (225 psia).

The results for the fuel air ratio of 0.01 (Table. 5) are shown first. As can be seen, rake temperatures tend to increase with percent FT fueling.

The CFD temperature contour through the centerline of the middle nozzle is shown in Fig. 6, which shows similar thermal characteristics. Thermal isopleths illustrate flame structure, Fig. 7

left figure, which is compared to an experimental photograph on the right by use of 0% FT.

Figure 8 shows the static pressure contour for 0% FT. Contours for 50% and 100% FT are similar.

The results for the fuel:air ratio of 0.015 are shown in Table. 6 and Fig. 9, with the exception that the rake exit temperature is questionable and most likely due to an open thermocouple.

The results for the fuel:air ratio of 0.02 are shown in Table. 7 and Fig. 10, with Fig. 11 illustrating a visual comparison of flame luminosity changes with percent FT fueling.

These data illustrate an increase in rake temperatures with percent FT fueling and fuel:air ratio which tends to shift the flame toward the upper wall of the combustor. Such trends may affect the combustor liner life and require further investigation.

CONCLUSIONS

The simplified two-parameter form of the gas phase caloric equations generated by use of the Planck-Einstein relation for C_p^0, the NIST REFPROP thermophysical property code, and the NASA McBride thermodynamic properties code, along with a systematic curve-fitting methodology established in Brankovic (2007) provide a basis for blended fuel thermophysical properties necessary for an established computational fluid dynamics (CFD) flow solver combustor code.

Computed flow structure and thermal profiles for synthetic (S8) fuel blended with JP-8 at 0% S8, at 50% S8 and 50% JP-8, and at 100% S8 using combustor A experimental rig as a test case show strong similarities.

Inspection of the mass-averaged combustor exit rake temperatures at fuel/air ratios of 0.010, 0.015, and 0.020 indicate that rake temperature differences increase with percentage S8 fueling and may be sufficient to require reconsideration of turbine fueling schemes.

REFERENCES

Brankovic, A., Ryder, R. C., Hendricks, R. C., and Huber, M. L., 2007, "A Step Toward CO_2-Neutral Aviation," SAE Paper 07ATC–214, *2007 SAE AeroTech Congress & Exhibition*, Los Angeles, CA (see also NASA/TM—2008-214998 http://gltrs.grc.nasa.gov/reports/2008/TM-2008-214998.pdf).

Brankovic, A., Ryder, R. C.; Hendricks, R. C., Liu, Nan-Suey, Shouse, D. T., and Roquemore, W. M., 2005, "Emissions Prediction and Measurement for Liquid Fueled TVC Combustor With and Without Water Injection," AIAA−2005−0215, AIAA, Reston, VA.

Hendricks, R. C., Shouse, D. T., Roquemore, W. M., Burrus, D. L., Duncan, B. S., Ryder, R. C., Brankovic, A., Liu, N.-S., Gallagher, J. R., and Hendricks, J. A., 2001, "Experimental and Computational Study of Trapped Vortex Combustor Sector Rig With High-Speed Diffuser Flow," Int. J. Rotating Machinery, Vol. 7, No. 6, 2001, pp. 375–385.

Hendricks, R. C., Ryder, R. C., Brankovic, A., Shouse, D. T., Roquemore, W. M., and Liu, N.-S., 2004, "Computational Parametric Study of Fuel Distribution in an Experimental Trapped Vortex Combustor Sector Rig," ASME GT2004–53225, ASME, New York, NY.

Huber, M. L., 2007, "NIST Thermophysical Properties of Hydrocarbon Mixtures Database: Version 3.2," NIST Standard Reference Database 4, National Institute of Standards and Technology, Gaithersburg, MD.

Huber, M. L., Lemmon, E. W., Diky, V., Smith, B. L., and Bruno, T. J., 2008a, "Chemically Authentic Surrogate Mixture

Model for the Thermophysical Properties of a Coal-Derived-Liquid Fuel," *Energy & Fuels*, Vol. 22, pp. 3249–3257.

Huber, M. L., Lemmon, E. W., Kazakov, A., Ott, L. S., and Bruno, T. J., 2009, "Model for Thermodynamic Properties of a Biodiesel Fuel," *Energy & Fuels*, Vol. 23, pp. 3790–3797.

Huber, M. L., Smith, B. L., Ott, L. S., and Bruno, T. J., 2008b, "Surrogate Mixture Model for the Thermophysical Properties of Synthetic Aviation Fuel S–8: Explicit Application of the Advanced Distillation Curve," *Energy & Fuels*, Vol. 22, No. 2, pp. 1104–1114. http://pubs.acs.org/doi/full/10.1021/ef700562c

Lemmon, E. W., Huber, M. L., McLinden, M. O., 2009, "REFPROP: Reference Fluid Thermodynamic and Transport Properties," NIST Standard Reference Database 23, Version 8.1beta.

McBride, B. J., Zehe, M. J., and Gordon, S., 2002, "NASA Glenn Coefficients for Calculating Thermodynamic Properties of Individual Species," NASA/TP—2002-211556, NASA Glenn Research Center, Cleveland, OH.

Molnar, M., and Marek, C. J., 2003, "Reduced Equations for Calculating the Combustion Rates of Jet-A and Methane Fuel," NASA/TM—2003-212702, NASA Glenn Research Center, Cleveland, OH.

Yokozeki, A., Sato, H., and Watanabe, K., 1998, "Ideal-Gas Heat Capacities and Virial Coefficients of HFC Refrigerants," *International Journal of Thermophysics*, Vol. 19, No. 1.

Table. 1 Simulated S8 components
and their mole fractions

Pure component	Mole fraction
n-nonane	0.03
2,6-dimethyloctane	0.28
3-methyldecane	0.34
n-tridecane	0.13
n-tetradecane	0.2
n-pentadecane	0.015
n-hexadecane	0.005

Table. 2 Planck-Einstein equation coefficients for S8 C_p^0 J/(mol-K)

Pure component	C_0	C_1	C_2	C_3	C_4	C_5	C_6	C_7
n-nonane	27.5016	0.328801	45.8854	1611.82	188.931	1611.84	53.2937	3132.19
2,6-dimethyloctane	13.6177	0.431076	190.612	1102.12	0.272831	1102.12	159.192	2368.26
3-methyldecane	52.9168	0.205539	203.245	1089.69	252.926	2173.08	100.168	5771.39
n-tridecane	50.4036	0.279146	338.515	1534.36	103.734	2780.47	0	0
n-tetradecane	72.2898	0.225453	352.454	1500.87	143.939	2385.49	0	0
n-pentadecane	43.7974	0.314173	25.8521	208.538	387.805	1554.14	97.0835	2669.68
n-hexadecane	32.4829	0.02306	418.705	1327.74	235.792	178.053	335.57	2585.74

Table. 3 Two-parameter model constants[a] (Eqs. (8) and (9))

Fluid	C/H ratio	Molecular mass	A	B	C_1	C_2
JP-10[b]	10/16	136.24	−1442.3	99.597	9481.8	−691.42
Synthetic	10.653/23.306	151.4	−1671.8	120.68	−6983.8	−808.36
Jet A	12/23	167.31	−1786	133.75	−8392.8	−893.608
			A'	B'	C_1'	C_2'
S8 (dimensional)	13.63/29.53	164.79	−15202	1097.8	191400	−7960

[a]Uncertainties in two-parameter model A and B result in C_p^0 within ±5%, H^0 within ±3%, and S^0 within ±2% to 3%.

[b]Exo-tetrahydrodicyclopentadiene.

Table. 4 Liquid-phase fuel properties for synthetic CTL and S8 GTL used in CFD code

Fuel	Molecular weight	Boiling point at 0.1MPa (K)	Density at 298 K (kg/m^3)	Density at boiling point (kg/m^3)	Latent heat (kJ/kg)	Specific heat (kJ/(kg-K))	Thermal conductivity (mW/(m-K))	Viscosity (μPa-s)
Synthetic	151.4	447.2	747	614.6	290	2.75	96	226
S8	164.79	457.33	736.8	611.5	339	2.793	93.5	227.5

Table. 5a Results for Combustor A,[a] fuel:air ratio = 0.01, 0% FT

	% Pressure loss	Exit temperature, top rake (K (°F))	Exit temperature, middle rake (K (°F))	Exit temperature, bottom rake (K (°F))
Experiment	9.44	1149 (1608)	1190 (1682)	1095 (1511)
CFD	9.29	1158 (1624)	1133 (1579)	1095 (1512)
% Difference	2.33	−0.995	6.12	−0.0662

Table. 5b Results for Combustor A,[a] fuel:air ratio = 0.01, 50% FT

	% Pressure loss	Exit temperature, top rake (K (°F))	Exit temperature, middle rake (K (°F))	Exit temperature, bottom rake (K (°F))
Experiment	9.54	1172 (1659)	1204 (1708)	1076 (1477)
CFD	9.28	1159 (1627)	1206 (1712)	1104 (1527)
% Difference	2.73	1.93	−0.234	−3.39

Table. 5c Results for Combustor A,[a] fuel:air ratio = 0.01, 100% FT

	% Pressure loss	Exit temperature, top rake (K (°F))	Exit temperature, middle rake (K (°F))	Exit temperature, bottom rake (K (°F))
Experiment	9.00	1209 (1717)	1218 (1733)	1093 (1508)
CFD	9.27	1194 (1689)	1231 (1756)	1104 (1573)
% Difference	−3.0	1.63	−1.33	−4.31

[a]Uncertainties in all CFD computations asserts that experimental data are correct, and % Difference represents uncertainty in CFD analysis. Experimental uncertainty is not addressed herein.

Table. 6a Results for Combustor Aa[a] fuel:air ratio = 0.015, 0% FT

	% Pressure loss	Exit temperature, top rake (K (°F))	Exit temperature, middle rake (K (°F))	Exit temperature, bottom rake (K (°F))
Experiment	9.29	[b]1809 (2797)	1384 (2032)	1270 (1827)
CFD	9.24	1634 (2482)	1450 (2150)	1239 (1771)
% Difference	0.538	11.3	−5.81	3.07

Table. 6b Results for Combustor A,[a] fuel:air ratio = 0.015, 50% FT

	% Pressure loss	Exit temperature, top rake (K (°F))	Exit temperature, middle rake (K (°F))	Exit temperature, bottom rake (K (°F))
Experiment	9.27	[b]1809 (2797)	1419 (2094)	1297 (1875)
CFD	9.25	1639 (2490)	1503 (2245)	1253 (1795)
% Difference	0.216	11.0	−7.21	4.27

Table. 6c Results for Combustor A, fuel:air ratio = 0.015, 100% FT

	% Pressure loss	Exit temperature, top rake (K (°F))	Exit temperature, middle rake (K (°F))	Exit temperature, bottom rake (K (°F))
Experiment	9.17	[b]1809 (2797)	1433 (2119)	1331 (1936)
CFD	9.23	1653 (2515)	1511 (2261)	1300 (1880)
% Difference	−0.654	10.1	−6.70	2.89

[a]Uncertainties in all CFD computations asserts that experimental data are correct, and % Difference represents uncertainty in CFD analysis. Experimental uncertainty is not addressed herein.

Table. 7a Results for Combustor A,[a] fuel:air ratio = 0.02, 0% FT

	% Pressure loss	Exit temperature, top rake (K (°F))	Exit temperature, middle rake (K (°F))	Exit temperature, bottom rake (K (°F))
Experiment	9.62	[b]1809 (2797)	1582 (2388)	1495 (2231)
CFD	9.28	1701 (2603)	1603 (2425)	1511 (2260)
% Difference	3.53	6.94	−1.55	−1.30

Table. 7b Results for Combustor A,[a] fuel:air ratio = 0.02, 50% FT

	% Pressure loss	Exit temperature, top rake (K (°F))	Exit temperature, middle rake (K (°F))	Exit temperature, bottom rake (K (°F))
Experiment	9.24	[b]1809 (2797)	1561 (2350)	1453 (2155)
CFD	9.27	1752 (2694)	1567 (2361)	1538 (2309)
% Difference	−0.325	3.68	−0.468	−7.15

Table. 7c Results for Combustor A,[a] fuel:air ratio = 0.02, 100% FT

	% Pressure loss	Exit temperature, top rake (K (°F))	Exit temperature, middle rake (K (°F))	Exit temperature, bottom rake (K (°F))
Experiment	9.20	[b]1809 (2797)	1584 (2391)	1506 (2251)
CFD	9.29	1751 (2692)	1550 (2330)	1523 (2281)
% Difference	−0.978	3.75	2.55	−1.33

[a]Uncertainties in all CFD computations asserts that experimental data are correct, and % Difference represents uncertainty in CFD analysis. Experimental uncertainty is not addressed herein.
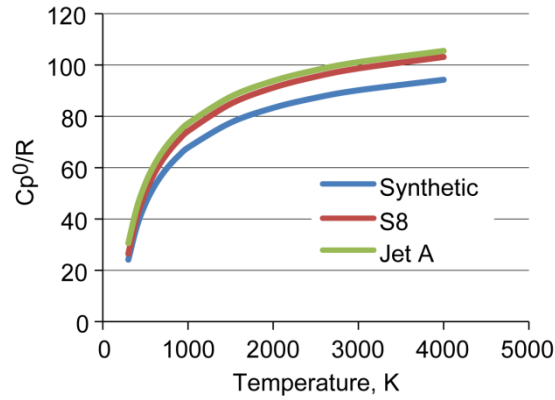[b]Questionable thermocouple.

Fig. 1a C_p^0/R for Synthetic CTL (coal-to-liquid),
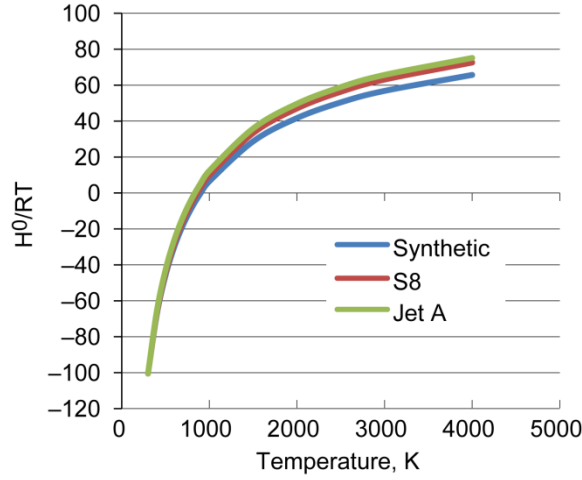S8 GTL (gas-to-liquid), and Jet A

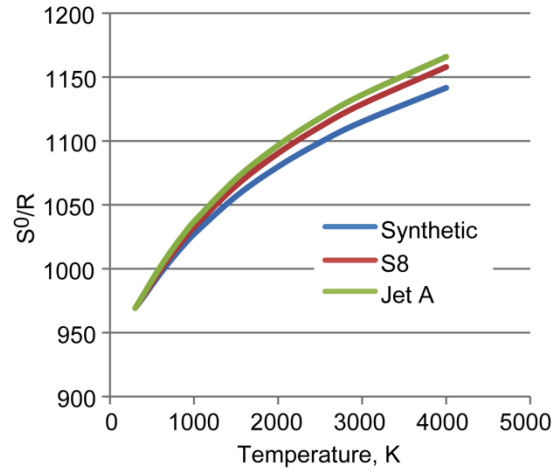Fig. 1b $H^0/(RT)$ for synthetic CTL, S8 GTL, and Jet A, with reference H^{00} set to Jet A-1 at 300 K

Fig. 1c S0/R for synthetic CTL, S8 GTL, and Jet A, with reference S00 set to Jet A-1 at 300 K
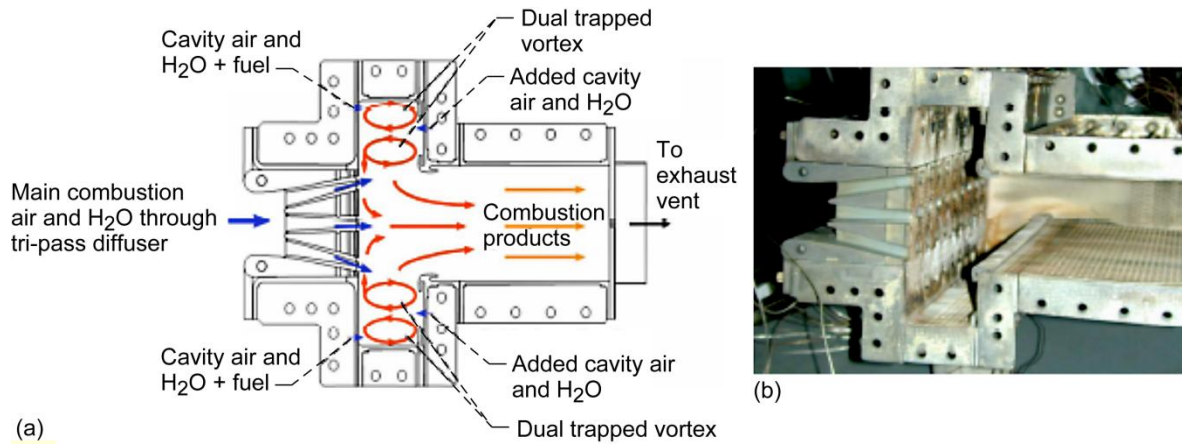

Fig. 2a Trapped vortex combustor (TVC). Arrows indicate major flow components. Liquid fuel is injected into TVC cavity and also directly into main combustor through orifices in diffuser. 2b Test rig hardware for TVC, with near sidewall removed for optical access. Photograph shows 10 fuel injector modules in spanwise direction. From NASA/TM—2008-214998 (see Brankovic et al., 2007)
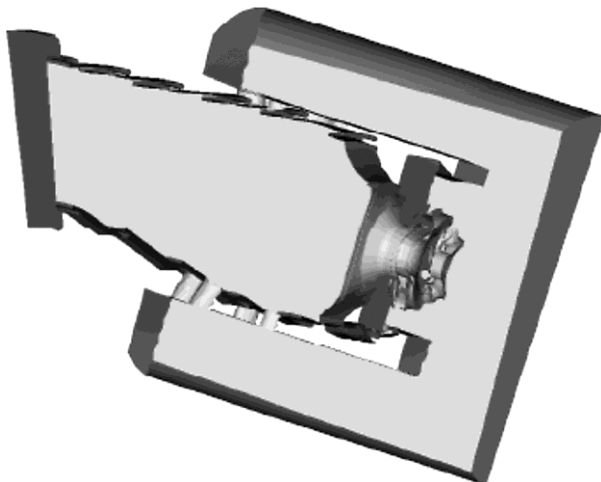
8

Fig. 3 Single combustion section cut in half down the fuel nozzle centerline with added external surround feed plenum
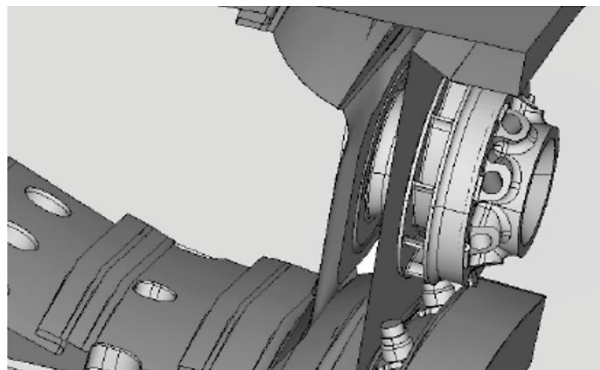

Fig. 4 Side view of fuel nozzle illustrates the swirling core air holes and secondary counter-swirling air vanes
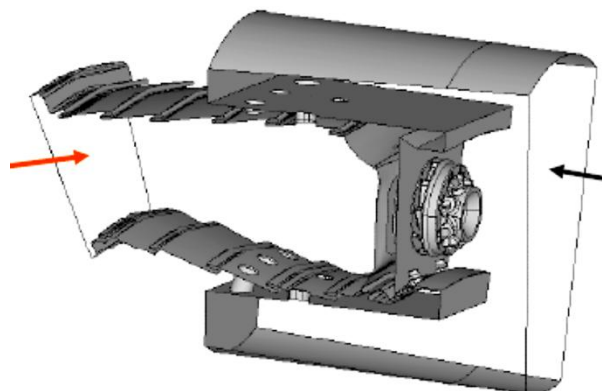

Fig. 5 One of the three combustion sections of AFRL/WPAFB test sector: (i) total air flow into the sector (black arrow), (ii) exit pressure at the sector exit plane (red arrow), and (iii) fuel droplet specification (not shown)

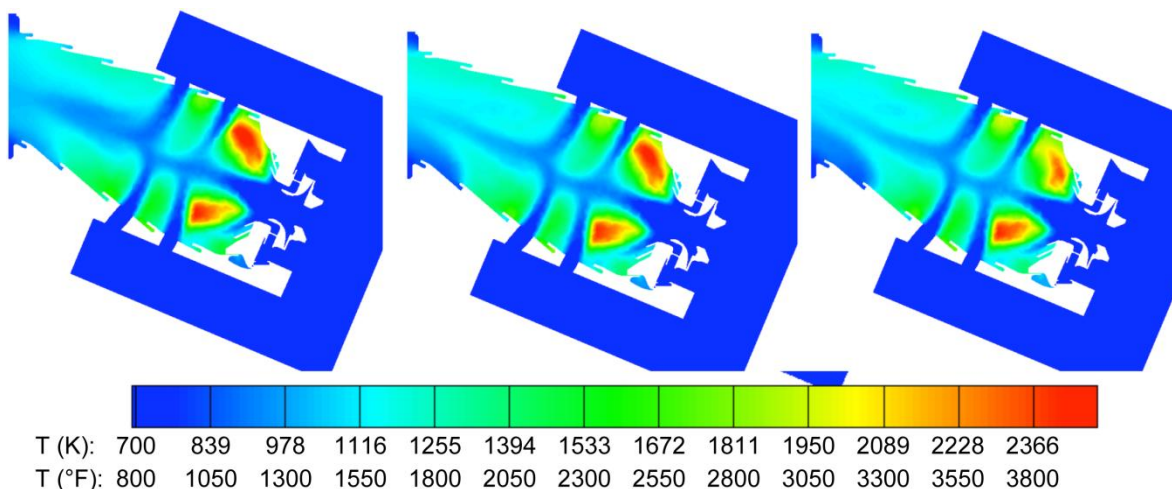| T (K): | 700 | 839 | 978 | 1116 | 1255 | 1394 | 1533 | 1672 | 1811 | 1950 | 2089 | 2228 | 2366 |
| T (°F): | 800 | 1050 | 1300 | 1550 | 1800 | 2050 | 2300 | 2550 | 2800 | 3050 | 3300 | 3550 | 3800 |

Fig. 6 Combustor A center plane temperature contours in °F. Inlet pressure 225 psia (1.55 MPa). Fuel:air ratio is 0.01. Left contour is 0% FT, center contour is 50% FT, and the right contour is 100% FT
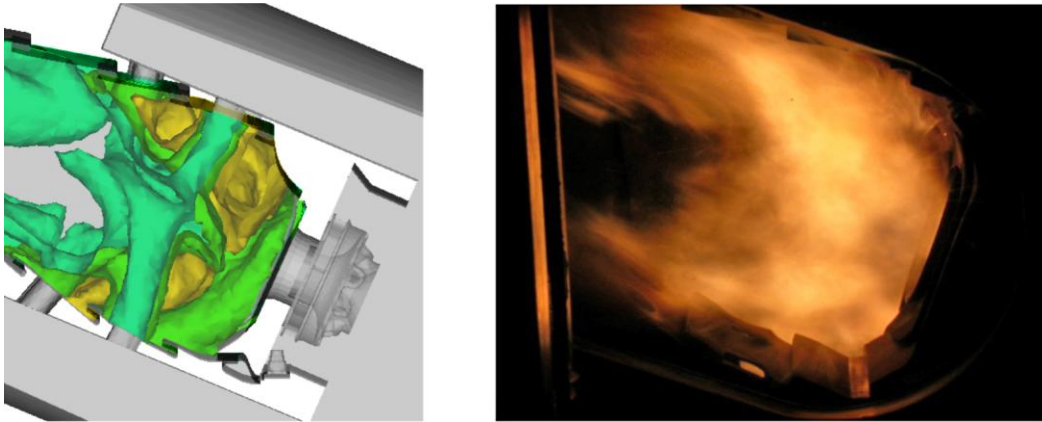
Fig. 7 Combustor A CFD temperature isopleths (flame structure) shown to the left compared with experiment
photograph to the right using 0% FT.

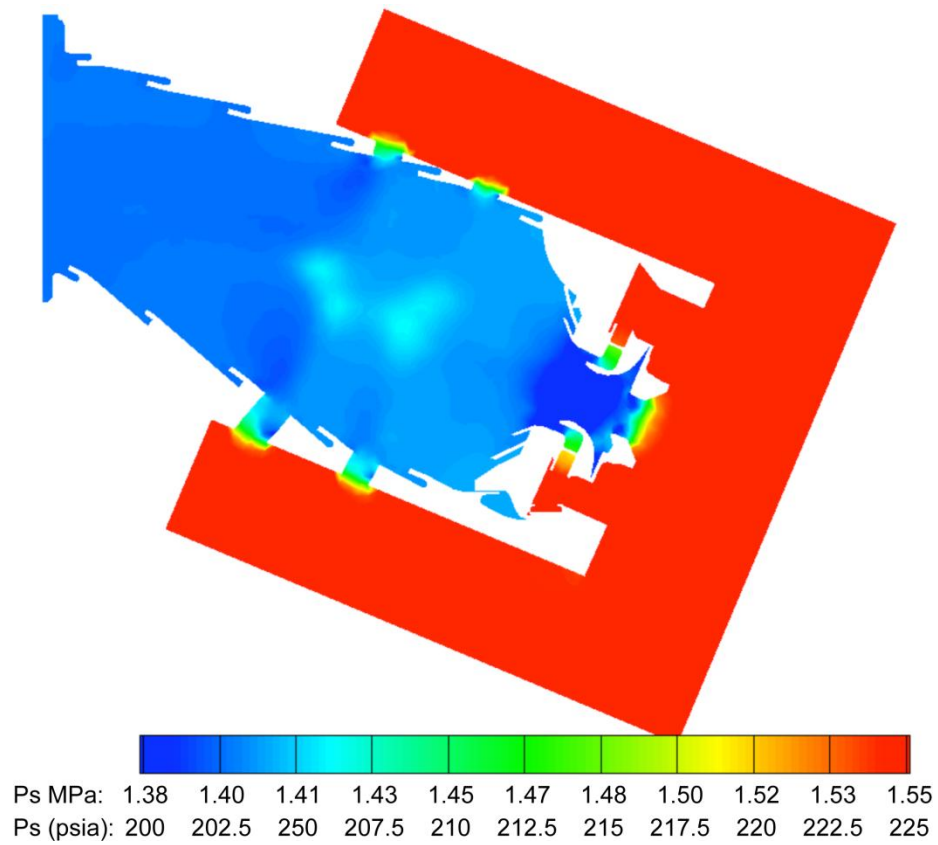| Ps MPa:	1.38	1.40	1.41	1.43	1.45	1.47	1.48	1.50	1.52	1.53	1.55
Ps (psia):	200	202.5	250	207.5	210	212.5	215	217.5	220	222.5	225

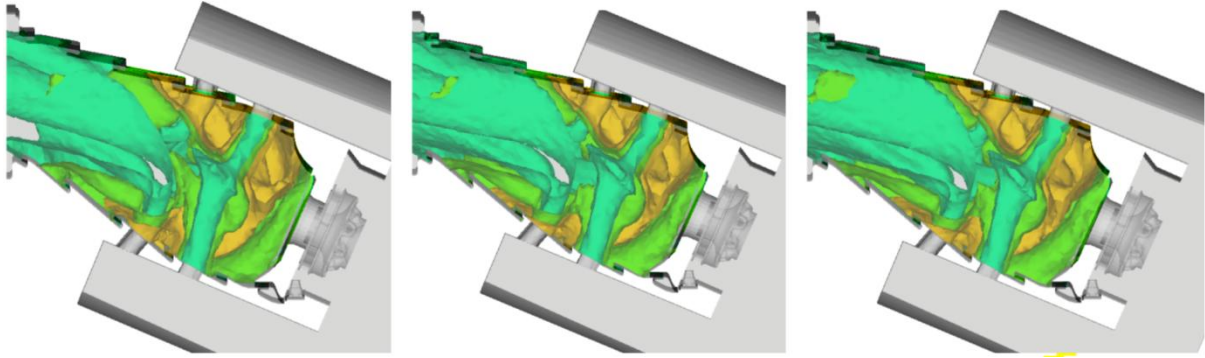Fig. 8 Static pressure contour (Ps) for Combustor A, 0% FT.

Fig. 9 Combustor A CFD temperature isopleths (flame structure) shown for Combustor A at fuel:air ratio of 0.015. Left is 0% FT, center is 50% FT, and right is 100% FT.
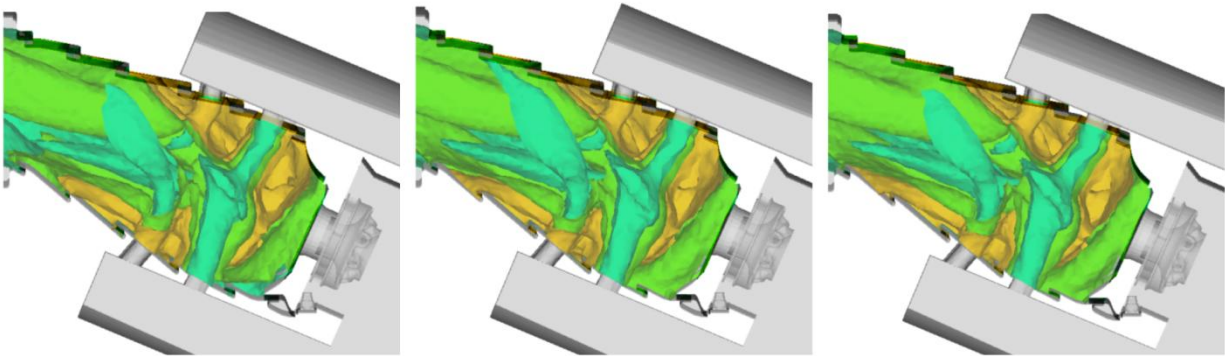

Fig. 10 Combustor A CFD temperature isopleths (flame structure) shown for fuel:air ratio of 0.02. Left is 0% FT, center is 50% FT and right is 100% FT
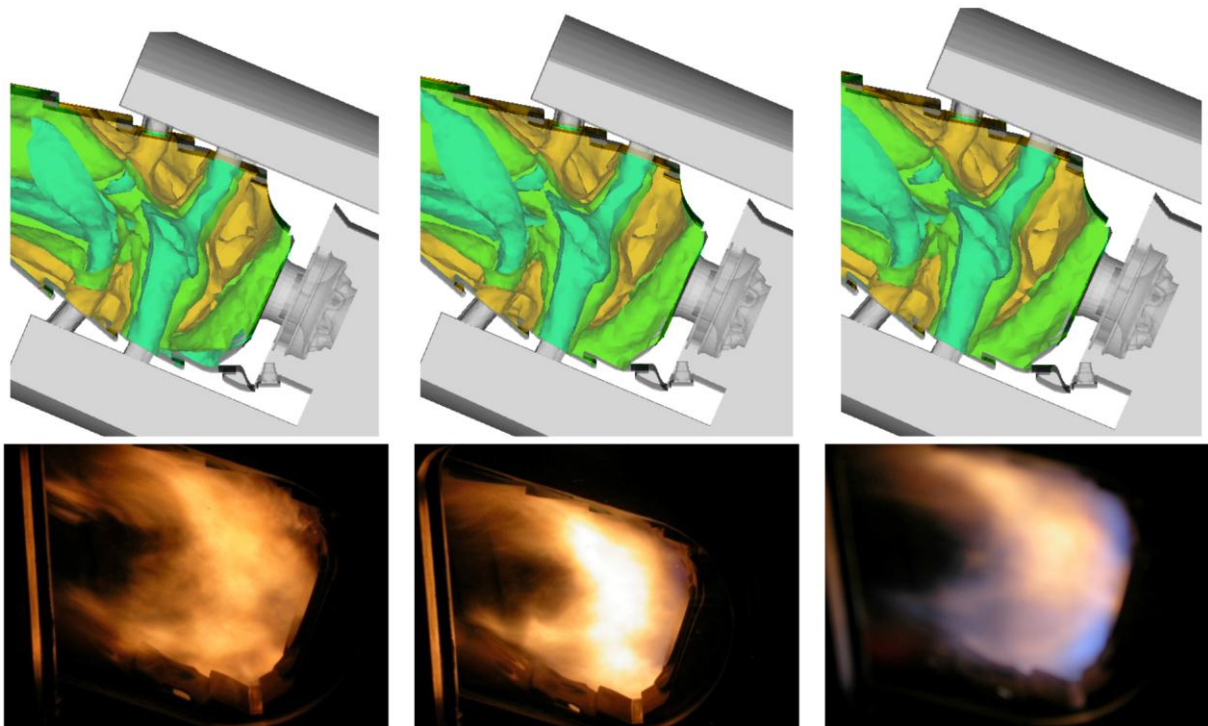

Fig. 11 Combustor A experiment photographs (flame structure) shown in bottom row; CFD temperature isopleths shown in top row. Left is 0% FT, center is 50% FT, and right is 100% FT.

APPENDIX

    For convenience, Tables. 1–4 in this Appendix are taken from NASA/TM—2008-214998 (see Brankovic et al., 2007), and Table. 4a is added to reflect actual values Brankovic et al. used in the CFD computations. Thermophysical and transport properties herein are based on STRAPP (Huber, 2007) with small differences from those that are predicted by REFPROP (Lemmon et al., 2009). At that time, it was not envisioned that a multitude of fuel designations, differences, or opinions would ensue complicating the names used in published literature.

    Table. 1: JP-8 Simulant for petroleum-based JP-8; in Tables of Brankovic et al., labeled JP-8

    Table. 2: Simulant for synthetic kerosene based on either CTL or GTL feedstock. The first formations of the synthetic fuels to become designated as SPK.

    Table. 3: Theromphysical property parameter coefficients for gaseous JP-8 petroleum-based stimulant, simulant for synthetic kerosene, and blends; in Tables of Brankovic et al., labeled JP-8, JP-8, Synthetic, and blends

    Table. 4: Liquid phase properties of Brankovic et al., again JP-8 labeled, JP-8, Synthetic, and blends

    Table. 4a: Thermophysical property values available to Brankovic et al. CFD code

Table. A1 JP-8 simulant components and fractions used as input to NIST hydrocarbon data base STRAPP (Huber, 2007)

JP-8 component		Mass fraction	Mole fraction	Molecular weight	Mass/weight
2,2,4-trimethylpentane (isooctane)	224TMP	0.0500	0.0640	114.22	0.000437752
Methylcyclohexane	MCC6	.0500	.0745	98.19	.000509217
meta-xylene	MXYL	.0500	.0688	106.17	.000470943
Cyclooctane	CC8	.0500	.0652	112.22	.000445553
n-decane	C10	.1500	.1542	142.28	.001054259
Butylbenzene	C4BNZ	0.0500	0.0545	134.22	0.000372523
1,2,4,5-tetramethylbenzene	1245TMBNZ	.0500	.0652	112.2	.000445633
1,2,3,4-tetrahydronaphthalene (tetralin)	TETRALIN	.0500	.0553	132.2	.000378215
n-dodecane	C12	.2000	.1717	170.34	.001174122
1-methylnaphthalene	1MNAPH	0.0500	0.0514	142.2	0.000351617
n-tetradecane	C14	.1500	.1106	198.39	.000756086
n-hexadecane	C16	.1000	.0646	226.45	.000441599
Mixture (JP–8 simulant)		1.0000	1.0000	[a]146.25 [b]146.25	0.006837519
STRAPP output				147.8	

[a]Value based on mass fraction.

[b]Value based on mole fraction.

Table. A2 Syntroleum corporation simulant components and fractions used as input to NIST hydrocarbon database STRAPP (Huber, 2007)

Syntroleum component		Mass fraction	Mole fraction	Molecular weight	Mass/weight
n-octane	C8	0.0430	0.0570	114.22	0.000376466
n-nonane	C9	.1000	.1181	128.26	.000779666
n-decane	C10	.1870	.1990	142.28	.00131431
n-undecane	C11	.1900	.1841	156.31	.001215533
n-dodecane	C12	.1320	.1174	170.34	.000774921
n-tridecane	C13	0.0930	0.0764	184.36	0.000504448
n-tetracecane	C14	.0740	.0565	198.39	.000373003
n-pentadecane	C15	.0270	.0192	212.42	.000127107
3-methyloctane	3MO	.0720	.0850	128.26	.00056136
2-methylnonane	2MN	.0820	.0873	142.29	.000576288
Mixture (Syntroleum simulant)		1.0000	1.0000	[a]151.44 [b]151.44	0.006603101
STRAPP output				151.4	

[a]Value based on mass fraction.

[b]Value based on mole fraction.

Table. A3 Carbon-to-hydrogen ratios (C/H), molecular weights (MW), and constants for Eqs. (8) through (10) used in simplified extrapolation method for investigated fuels

Fuel	Input for simplified extrapolation method					
	C/H	MW	A	B	C_1	C_2
JP-8	10.605/20.15	147.83	−1542.6	110.9	−314.83	−746.54
JP-8 (70%)/synthetic (30%)	10.629/21.72	148.94	−1582.4	113.9	−2321.47	−763.57
JP-8 (50%)/synthetic (50%)	10.620/21.09	149.60	−1607.3	115.8	−3673.2	−775.93
Synthetic	10.653/23.306	151.40	−1671.8	120.68	−6983.8	−808.36

Table. A4 Liquid-phase fuel properties for investigated fuels

Fuel	Liquid-phase fuel properties[a]				
	Molecular weight	Boiling point at 0.1 MPa (K)	Density at 298 K (kg/m^3)	Density at boiling point[b] (kg/m^3)	Latent heat (kJ/kg)
JP-8	147.83	436.3	800.7	681.7	255.0
JP-8 (70%)/synthetic (30%)	148.94	439.6	783.6	660.5	287.0
JP-8 (50%)/synthetic (50%)	149.6	441.7	772.8	647.0	296.0
Synthetic	151.4	447.2	747.0	614.6	290.0

[a]Isothermal flash properties (from NIST (Huber, 2007)).
[b]One or two components may be in solid phase.

Table. A4a Thermophysical properties available to Branckovic et al. CFD code simulations, based on values from STRAPP (Huber, 2007).

Fuel	Liquid-phase fuel properties[a]					
	Molecular weight	Boiling point at 0.1 MPa (K)	Density at 298 K (kg/m^3)	Latent heat (kJ/kg)[c]	Specific heat,[d] C_p^0 (kJ/kg-K)	Thermal conductivity,[d] λL (mW/m-K)
JP-8	147.83	436.3	800.7	285	1.95	134
JP-8 (70%)/Synthetic (30%)	148.94	441.7	784	286	2.01	134
JP-8 (50%)/Synthetic (50%)	149.6	440.1	772.8	297	2.01	134
Synthetic	151.4	447.7	744.9	288	2.01	134

[a]Isothermal flash properties (from NIST (Huber, 2007)).
[b]One or two components may be in solid phase.
[c]Bubble to dew point enthalpy difference at 1 bar.